Journal of Molecular Structure 1106 (2016) 430–439

Contents lists available at ScienceDirect

Journal of Molecular Structure

journal homepage: http://www.elsevier.com/locate/molstruc

Click one pot synthesis, spectral analyses, crystal structures, DFT studies and brine shrimp cytotoxicity assay of two newly synthesized 1,4,5-trisubstituted 1,2,3-triazoles

Muhammad Naeem Ahmed [a, **], Khawaja Ansar Yasin [a], Khurshid Ayub [b], Tariq Mahmood [b, *], M. Nawaz Tahir [c], Bilal Ahmad Khan [a], Muhammad Hafeez [a], Madiha Ahmed [d], Ihsan ul-Haq [d]

[a] Department of Chemistry, The University of Azad Jammu and Kashmir, Muzaffarabad, 13100, Pakistan
[b] Department of Chemistry, COMSATS Institute of Information Technology, University Road, Tobe Camp, 22060, Abbottabad, Pakistan
[c] Department of Physics, University of Sargodha, Sargodha, Pakistan
[d] Department of Pharmacy, Faculty of Biological Sciences, Quaid-i-Azam University, Islamabad, 54320, Pakistan

ARTICLE INFO

Article history:
Received 25 June 2015
Received in revised form
18 September 2015
Accepted 9 November 2015
Available online 14 November 2015

Keywords:
Click chemistry
Triazole
X-ray diffraction
DFT
Brine shrimp assay

ABSTRACT

Methyl-2-(1-benzyl-4-phenyl-1*H*-1,2,3-triazol-5-yl)-2-oxoacetate **(1)** and ethyl-2-(1-benzyl-4-phenyl-1*H*-1,2,3-triazol-5-yl)-2-oxoacetate **(2)** were synthesized by one pot three component strategy, and characterized by FT-IR, NMR (^{1}H and ^{13}C) spectroscopy and TOF-MS spectrometry. Finally, the structures were unequivocally confirmed by single crystal X-ray diffraction analyses. Both compounds, **1** and **2** exist in monoclinic crystal packing having space group $P2_1/n$ and $P2_1/c$, respectively. Crystal structures investigations revealed that the molecular structures of the title compounds are stabilized by weak intermolecular hydrogen bonding interactions to form dimers. Density functional theory (DFT) calculations were performed not only to compare with the experimental spectroscopic results but also to probe structural properties. The molecular electrostatic potential (MEP) mapped over the entire stabilized geometries of the molecules delivered information about the electrophilic and nucleophilic sites. Furthermore, frontier molecular orbital analysis gave the idea about stability and reactivity of compounds. Both compounds were also screened for brine shrimp cytotoxicity assay.

1. Introduction

Click chemistry has recently emerged as an important tool in synthetic chemistry [1]. In recent years, the design and synthesis of pharmacologically relevant heterocyclic molecules by combinatorial techniques is proven as a promising approach in the search for new pharmacological lead structures [2]. Click chemistry is one of the leading reactions to make carbon-heteroatom-carbon (C-X-C) bonds in aqueous environment. Structures bearing C-X-C moiety possess a wide variety of chemical and biological applications in various fields [3–6]. Click reactions require only benign reaction conditions, simple workup including purification procedures, and can still promptly create molecular diversity through the use of reactive modular building blocks. In search for new compounds through these reliable and efficient reactions, click chemistry may accelerate the process of discovery and optimization [3,7].

Importance and applications of triazole chemistry regarding the click reactions is not much hidden, and has been explored by the scientific community extensively [8]. Click chemistry has been successfully applied to synthesize compounds for drug discovery, enzyme inhibition, receptor-ligand binding studies, for DNA labeling and for studying the biological systems [1].

In continuation of our ongoing research regarding the synthesis of 1,4,5-trisubstituted 1,2,3-triazole [9] derivatives via click reaction and density functional theory studies of different classes [10–12], here we are reporting the synthesis, structural investigations and brine shrimp cytotoxic assay of two new 1,4,5-trisubstituted 1,2,3-triazoles. Both compounds were synthesized in good yields, characterized by spectroscopic analysis and finally, the structures were

* Corresponding author.
** Corresponding author.
E-mail addresses: aromatics790@gmail.com (M.N. Ahmed), mahmood@ciit.net.pk (T. Mahmood).

http://dx.doi.org/10.1016/j.molstruc.2015.11.010
0022-2860/

confirmed unambiguously by X-ray diffraction studies. The DFT simulations were performed not only to validate the spectroscopic results, but also to investigate other structural properties like frontier molecular orbital (FMOs) analysis, molecular electrostatic potential (MEP). Both compounds were also screened for their brine Shrimp cytotoxicity assay.

2. Materials and methods

2.1. Experimental

Different alkyl and aryl azides were purchased from *J* and *K* chemicals China, and were used without further purification. Phenylacetylides were prepared according to the procedures reported in the literature [13]. Solvents of analytical reagent (AR) grades were purchased from Sigma Aldrich, and used without purification. Melting points were determined on a Yanaco melting point apparatus, and are reported as uncorrected. Thin layer chromatography (TLC) was carried out using pre coated silica gel 60 HF254 aluminum sheets (Merck). IR spectra were recorded on a Nicolet FT-IR 5DX spectrometer, using ATR method. The ^{1}H NMR (300 MHz) and ^{13}C NMR (75 MHz) spectra were recorded in $CDCl_3$ on a JEOL JNM-ECA 300 spectrometer. TMS was used as an internal reference and *J* values were calculated in Hz. HR-MS were obtained on a Bruker microTOF-QII spectrometer.

2.2. Synthesis

The synthesis of triazole derivatives (**1** and **2**) was carried out by adopting click one pot three component synthetic methodology (for synthetic scheme see Fig. 1).

2.2.1. General procedure for the synthesis of triazoles *1* and *2*

Synthesis of both compounds was accomplished by slight modification of the procedure already described in the literature [9,14].

Methoxalyl chloride for compound **1** and ethoxalyl chloride for compound **2** (0.07 g, 0.5 mmol) was added to a suspension of benzylazide (0.08 g, 0.6 mmol), copper (1) phenylacetylide (0.09 g, 0.5 mmol) and chlorobenzene (2 ml). The resultant mixture was stirred at room temperature for 4 h, and finally subjected to flash column chromatography eluting with 10% ethylacetate in petroleum ether to obtain **1** and **2** as white solids.

*2.2.1.1. Methyl 2-(1-benzyl-4-phenyl-1H-1,2,3-triazol-5-yl)-2-oxoacetate **(1)**.* White crystalline solid, m. p. 75–77 °C, Yield = 91%, **IR** (ATR, cm^{-1}): ν_{max} 3031 ($CH_{arom.}$), 2954 (CH), 1739 ($COOCH_3$), 1687 (C=O), 1484 (C=C), 1455 (C=C), 1220 (N=N); **^{1}H-NMR** δ ppm 7.50–7.30 (m, 10H), 5.90 (s, 2H), 3.29 (s, 3H); **^{13}C-NMR** δ ppm 176.9, 161.2, 153.2, 134.2, 129.7, 129.5, 129.0, 128.8, 128.6, 128.5, 128.1, 127.2, 54.2, 52.7. **HRMS** (ESI-TOF) (*m/z*): calculated for $C_{18}H_{15}N_3O_3$, $[M+H]^+$ 322.1186; observed 322.1187.

*2.2.1.2. Ethyl 2-(1-benzyl-4-phenyl-1H-1, 2, 3-triazol-5-yl)-2-oxoacetate **(2)**.* White crystalline solid, m.p. 74–76 °C, Yield = 89%, **IR** (ATR, cm^{-1}): ν_{max} 3057 ($CH_{arom.}$), 2981 (CH), 1741 ($COOCH_3$), 1683 (C=O), 1537 (C=C), 1477 (C=C), 1224 (N=N); **^{1}H-NMR** δ ppm 7.52–7.28 (m, 10H), 5.88 (s, 2H), 3.71 (q, 2H, J = 7.2 Hz), 0.92 (t, 3H, J = 7.2 Hz); **^{13}C-NMR** δ ppm 177.3, 160.8, 152.9, 134.1, 129.6, 128.9, 128.7, 128.6, 128.5, 128.1, 127.2, 62.8, 54.1, 13.2. **HRMS** (ESI-TOF) (*m/z*): calculated for $C_{19}H_{17}N_3O_3$, $[M+H]^+$ 336.1343; observed 336.1345.

2.3. Crystallography

Suitable crystals of both compounds **1** and **2**, having proper size and shape were selected and analyzed by single crystal X-ray diffraction technique. Selected crystal of each compound was coated with paratone 8772 oil and mounted on a glass fiber. All measurements were made on Bruker Kappa *APEX*-IICCD diffractometer with graphite monochromatic M_o-K_α radiation. The structures were solved by direct method and refined by using *SHELXL* 2013 (Sheldrick, 2013) [15]. The figures were plotted with the aid of ORTEP II.

The cif files of both compounds have been assigned CCDC numbers 983913 and 994384 and can be obtained free of charge on application to CCDC 12 Union Road, Cambridge CB21 EZ, UK. (Fax: (+44) 1223 336-033; e-mail: data_request@ccdc.cam.ac.uk).

2.4. Computational details

Computational investigations were performed at density functional theory level by using Gaussian 09 software [16]. The visualization of the results/optimized geometries was achieved through GuassView 5.0 [17]. Optimization of both triazole derivatives **1** and **2** was carried out at B3LYP/6-31G (d, p) level of theory. Frequency simulations were performed at the same level, to confirm the optimized geometries as true minima (no imaginary frequency). Furthermore, frequency output files were used for simulated vibrational analysis. Theoretical nuclear magnetic resonance (^{1}H and ^{13}C NMR) studies were performed at B3LYP/6-311G+(2d,p) level, by adopting GIAO formalism, and the chemical shift were referred with reference to tetramethylsilane. Molecular electrostatic potential (MEP) and frontier molecular orbital (FMOs) were simulated at B3LYP/6-31G (d, p) level of DFT.

2.5. Brine shrimp cytotoxic lethality assay

A 24 h LC_{50} lethality test was performed in a 96 well plate using Brine shrimp (*Artemia salina*) larvae using literature method with some modifications [18]. Six graded concentrations (300, 100, 33.3, 11.1, 3.7, 1.3 μg/ml) in triplicate for test extracts were used.

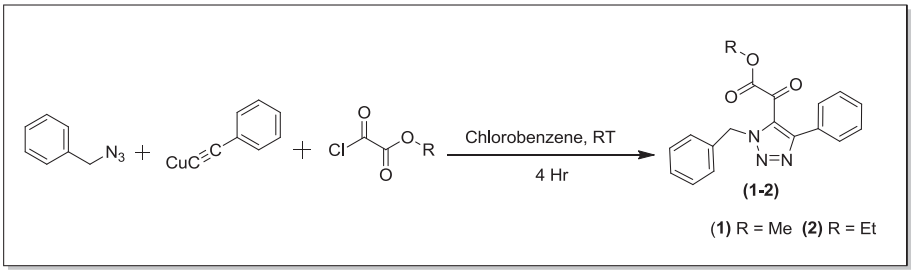

Fig. 1. Synthetic scheme for triazole derivatives **1** and **2**.

Doxorubicin was employed as reference standard and DMSO as negative control. Eggs of test organism *A. salina* Leach (Ocean 90, USA) were kept for hatching (48 h) in simulated sterile sea water with constant oxygen supply in a specially designed two-compartment plastic tray under a 60 W lamp, providing direct light and warmth (30–32 °C). The mature nauplii were then used for the cytotoxicity test and the number of survivors was counted after 24 h. Larvae were considered dead if they did not exhibit any internal or external movement during several seconds of observation. The median lethal concentration (LC_{50}) of the test samples was calculated using table curve 2D version 5.01 software.

3. Results and discussion

Both triazole based derivatives, methyl 2-(1-benzyl-4-phenyl-1*H*-1,2,3-triazol-5-yl)-2-oxoacetate **(1)** and ethyl 2-(1-benzyl-4-phenyl-1*H*-1,2,3-triazol-5-yl)-2-oxoacetate **(2)** were synthesized in good yields from commercially available starting materials by adopting one pot three component strategy (details have been naratted in the experimental section). After accomplishing the successful synthesis, the final structures were characterized by spectroscopic techniques like FT-IR, NMR (^{1}H and ^{13}C), and finally the structures were confirmed by single crystal X-ray diffraction studies.

3.1. X-ray diffraction analysis

Compounds **1** and **2** crystallized as white solid, and X-ray diffraction analysis was performed to ensure the final structures, and to study their three dimensional patterns. The complete crystal data parameters are narrated in (Table S1; supplementary information's) and *ORTEP* views of both **1** and **2** are shown in Fig. 2.

Both compounds are closely related to (*E*)-1-(benzyl-5-methyl-1*H*-1, 2, 3-triazol-4-yl)-3-phenylprop-2-en-1-one with different substitution on position 4 and 5 of the triazole ring [19,20]. The compound (**1**) consisting of benzyl, phenyl and methoxalyl moiety attached to the central 1, 2, 3-triazole ring crystallized in the monoclinic system having space group $P2_1/n$. Compound **2** which consists of benzyl, phenyl and ethoxalyl substituents attached to the 1,2,3-triazole ring also crystallized in same crystal system but with different space group $P2_1/c$. Packing diagrams of the title compounds showed that the molecules exist as dimers via several non-bonding interactions (Fig. 3). Packing patterns of compound **1** revealed that dimerization stabilized via H_7–O_1 hydrogen bonding whereas in **2** dimers linked via H_{19}–N_1 and O_3–H_9 hydrogen bonding interactions.

3.2. Geometry optimization

DFT is a valuable tool not only to compare and validate the experimental data, but also to look inside the structural properties of compounds. Both compounds (**1** and **2)** were optimized at B3LYP/6-31G (d, p) level to compare with the X-ray diffraction data (Fig. 4). Comparison of some important bond lengths and bond angles is given in Table 1 (bond lengths) and Table S2 (bond angles). Some important X-ray diffraction bond lengths in **1** such as O1–C16, O2–C17, O2–C18A, O3–C17, N1–N2, N1–C8, N1–C7, N2–N3 and N3–C9 found at 1.207 Å, 1.240 Å, 1.480 Å, 1.246 Å, 1.331 Å, 1.361 Å, 1.472 Å, 1.323 Å and 1.352 Å respectively, whereas the computed values of these bond lengths were depicted at 1.223 Å, 1.339 Å, 1.444 Å, 1.207 Å, 1.333 Å, 1.376 Å, 1.475 Å, 1.310 Å and 1.361 Å. Similarly, the X-ray diffraction values of some important bond lengths such as O1–C16, O2–C17, O3–C17, O3–C18, N1–N2, N1–C7, N2–N3, N3–C8 and N3–C9 in **2** are observed at 1.208 Å, 1.195 Å, 1.317 Å, 1.465 Å, 1.315 Å, 1.361 Å, 1.333 Å, 1.369 Å and 1.453 Å respectively. Simulated values of these bond lengths are 1.222 Å, 1.208 Å, 1.337 Å, 1.455 Å, 1.310 Å, 1.361 Å, 1.333 Å, 1.375 Å and 1.474 Å, respectively. Maximum deviation in computed and X-ray bond lengths of both triazole derivatives **1** and **2** observed in the range 0.002–0.099 Å and 0.00–0.034 Å respectively.

In **1**, X-ray values of some important bond angles such as C17–O2–C18A, N2–N1–C8, N2–N1–C7, C8–N1–C7, N3–N2–N1, N2–N3–C9, N1–C7–C1, N1–C8–C9, O1–C16–C8, O1–C16–C17, O2–C17–O3 and O2–C17–C16 are depicted at 116.0°, 110.3°, 118.5°, 131.1°, 108.2°, 108.7°, 112.3°, 104.5°, 123.4°, 118.6°, 126.2° and 117.6° respectively. These experimental values correlated nicely with theoretical ones appearing at 115.4°, 110.6°, 118.3°, 131.0°, 108.5°, 109.2°, 112.7°, 103.5°, 123.9°, 116.8°, 125.9° and 123.2° respectively. Similarly, the experimental and computed bond angles in **2** showed excellent correlation to each other (for individual values see Table S2). Maximum deviation in X-ray and computed bond angles of both compounds **1** and **2** observed in the range 0.1–5.6° and 0.0–3.3° respectively. After analyzing carefully the data, it is concluded that very good correlation exists between the X-ray and computed bond lengths and bond angle values.

3.3. Vibrational analysis

Experimental FT-IR spectra of triazole derivatives **1** and **2** were recorded by using ATR method, whereas simulated vibrational spectra were extracted from frequency calculation. Both experimental as well as simulated spectra are shown in Fig. S1

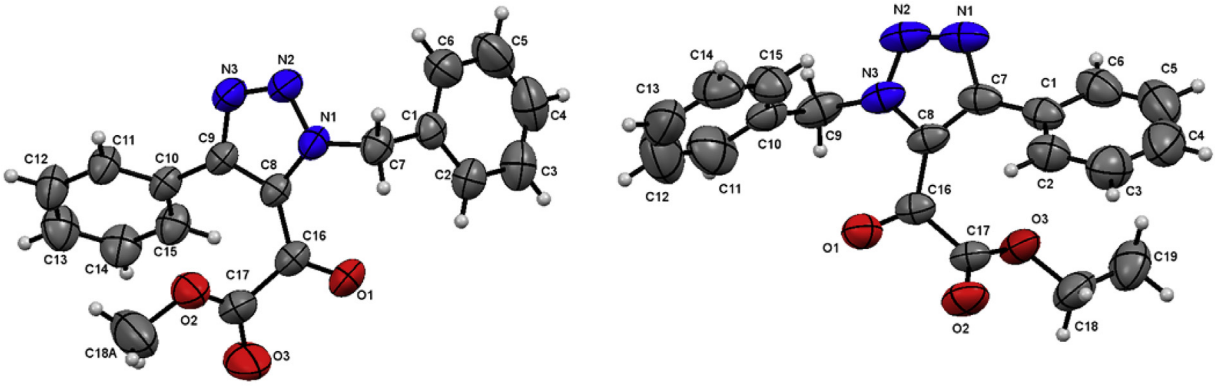

1 **2**

Fig. 2. *ORTEP* plot of compound (**1**) and (**2**) at 50% probability level. H-atoms are omitted for clarity purpose.

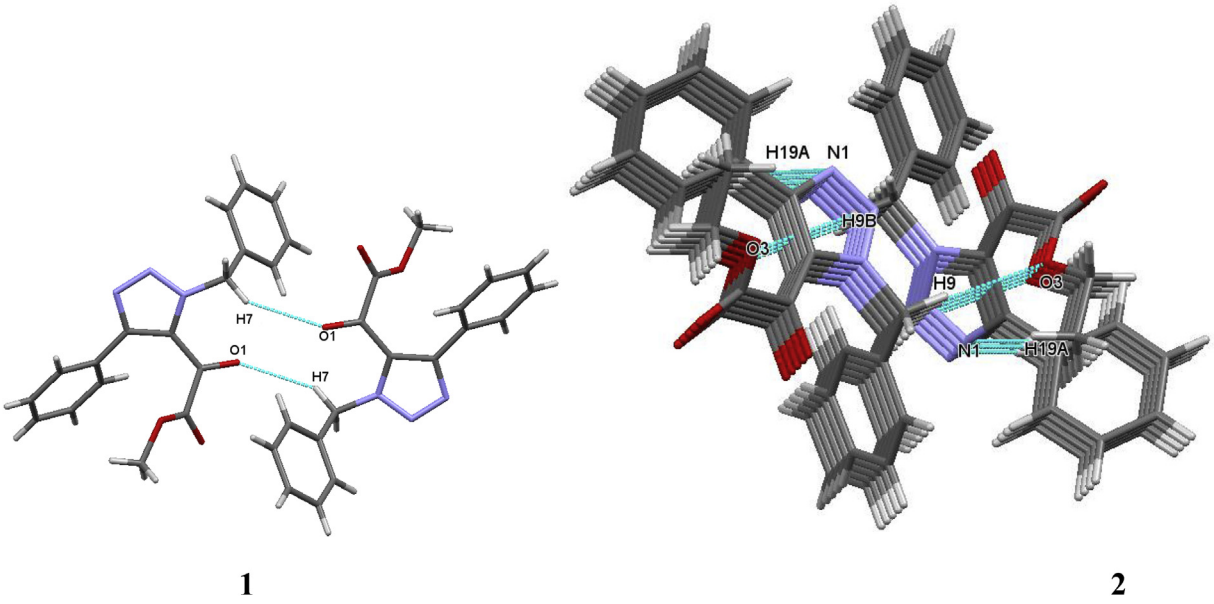

Fig. 3. Packing patterns of compound (**1**) showing dimers linked via H_7–O_1 and compound (**2**) showing dimers linked via H_{19}–N_1 and O_3–H_9.

(Supplementary information) and Fig. 5, respectively. Detailed comparison of experimental and calculated vibrational frequencies is narrated in Table 2. In order to minimize the theoretical error, simulated vibrations above 1700 cm^{-1} were scaled by using a scaling factor of 0.958 and for less than 1700 cm^{-1} scaling factor was 0.9627 [21]. Both compounds have mainly aromatic, carbonyl, ester, CH_2, and CH_3 functional groups. From Table 4, it is clear that there exists an outstanding agreement between the experimental and theoretical vibrations.

3.3.1. C=O vibrations

Among all functional groups, carbonyl is the one that can be easily identified by using vibrational spectroscopy, and experimentally a strong stretching vibration appears in the range 1650–1800 cm^{-1} [22]. The title compounds **1** and **2** have two different carbonyl functional groups, and their very strong stretching frequencies in simulated spectra appeared at 1755 cm^{-1} ($COOCH_3$), 1670 cm^{-1} (C=O) for **1**, and 1751 cm^{-1} (COOEt), 1671 cm^{-1} (C=O) for **2**. Experimental values of both carbonyl groups found at 1738 cm^{-1}, 1682 cm^{-1} for **1**, 1741 cm^{-1}, 1682 cm^{-1} for **2**, and coincide excellently with the computed values.

3.3.2. Aromatic vibrations

Low intensity aromatic (CH) stretching vibrations generally appear in the region 2800–3100 cm^{-1} [23]. In the simulated spectra, the prominent aromatic CH stretching (symmetric/asymmetric) vibrations of both **1** and **2** appeared in the range 3071–3062 cm^{-1}. These simulated aromatic CH stretching vibrations correlate nicely with the experimental values; 3031 cm^{-1} and 3057 cm^{-1} for **1** and **2**, respectively. The symmetric and asymmetric stretching vibrational region of aromatic ring (C=C) of medium intensity normally lies in the range of 1600–1200 cm^{-1} [24]. The simulated IR spectrum of **1** showed the aromatic C=C symmetric and asymmetric stretching vibrations at 1505 cm^{-1}, 1483 cm^{-1} 1467 cm^{-1} and 1434 cm^{-1}. Similarly the computed aromatic stretching C=C peaks of **2** appeared at 1513 cm^{-1}, 1483 cm^{-1}, 1467 cm^{-1} and 1434 cm^{-1}. The simulated aromatic C=C stretching vibrations showed strong agreement with their experimental counter parts depicted at 1484 cm^{-1}, 1455 cm^{-1} and 1431 cm^{-1} for compound **1**, and 1537 cm^{-1} and 1477 cm^{-1} for compound **2**.

3.3.3. CH_2 and Me group vibrations

The simulated stretching (symmetric/asymmetric) aliphatic CH vibrational frequency lie in the range of 2900–3100 cm^{-1} and these vibrations are usually weak due to less change in dipole moment. Both **1** and **2** showed simulated CH stretching vibrations in the range 3024–2943 cm^{-1} and 3015-2930 cm^{-1}, respectively. These simulated vibrations showed nice agreement with their experimental counterparts, at 2954 cm^{-1} for compound **1** and 3036 cm^{-1}, 2981 cm^{-1}, 2937 cm^{-1} for **2**. Other than stretching vibrations, several scissoring, in-plane and out of plane bending vibrations were observed for CH_2 and CH_3 groups of both **1** and **2**, in the simulated as well as experimental spectra and found in good agreement (for individual values see Table 4).

3.3.4. Triazole ring vibrations

Triazole ring is combination of C=N, N=N and C–N functional groups, and stretching vibrations of these groups lies in the range of 1200–1500 cm^{-1} [25]. Computed symmetric and asymmetric C=N stretching vibrations appeared at 1242 cm^{-1}, 1198 cm^{-1} for **1** and 1240 cm^{-1}, 1196 cm^{-1} for compound **2**. The experimental C=N stretching vibrations appeared at 1271 cm^{-1}, 1193 cm^{-1} (compound **1**) and 1262 cm^{-1}, 1201 cm^{-1} (compound **2**), respectively. Similarly, simulated as well as experimental N=N and C–N vibrations in both compounds showed an excellent correlation to each other. Very strong N=N symmetric stretching peak in the computed spectra of both compounds appeared at 1224 cm^{-1}, whereas respective experimental value was observed at 1220 cm^{-1} for **1** and 1224 cm^{-1} for **2**. Theoretical C–N stretching vibration of **1** was observed at 1312 cm^{-1} and for **2** at 1311 cm^{-1}, whereas experimental C–N vibration of both appeared at 1311 cm^{-1} (**1**) and 1333 cm^{-1} (**2**) simultaneously, and showed very good correlation.

3.4. Nuclear magnetic resonance (NMR) studies (^1H and ^{13}C)

Since last two to three decades, nuclear magnetic resonance spectroscopy has been used extensively for the structural elucidation of compounds. Besides the single crystal X-ray data, the ^1H and ^{13}C chemical shifts contain very important information about the structure of compounds. Nowadays, the DFT simulations are playing very active role to predict theoretical NMR chemical shifts and to compare with experimental results. Experimental NMR spectra

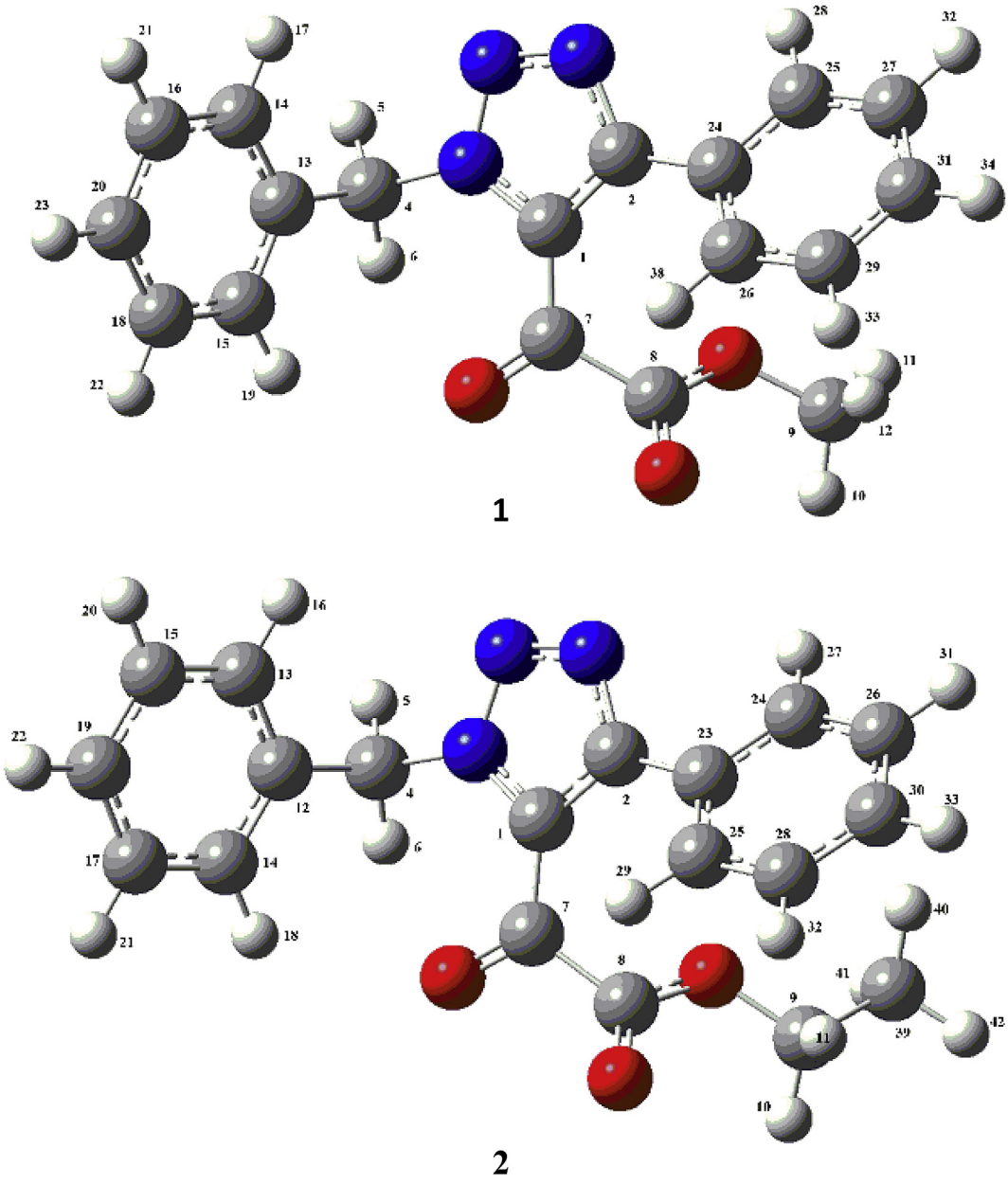

Fig. 4. Optimized geometries of **1** and **2** at 6-31G (d, p) level of DFT.

(both ^{1}H and ^{13}C) were recorded in $CDCl_3$, and are being shown in electronic supplementary information Fig. S2–S5. Simulated NMR spectra of both compounds **1** and **2** were computed by adopting GIAO method at B3LYP/6-311+G(2d,p) level of DFT. It is very well documented in the literature, that higher basis set works very well for accurate measurements of chemical shift values as compare to lower basis set [26]. The detailed comparison of simulated and experimental ^{1}H NMR chemical shifts of both compounds is narrated in Table 3.

Both compounds mainly have aromatic, CH_2 and CH_3 protons, in the experimental ^{1}H NMR spectrum, the aromatic protons appeared experimentally in the range 7.47–7.34 ppm (compound **1**) and 7.45–7.33 ppm (compound **2**), whereas computed aromatic C–H chemical shifts (with respect to TMS) appeared at 8.48–7.39 ppm (**1**)/8.59–7.40 (**2**) ppm. The methylene protons attached directly to the aromatic ring experimentally are depicted at 5.90 ppm and 5.88 ppm for **1** and **2**, respectively. The same protons in the simulated spectra appeared at 5.90–5.83 ppm (**1**)/5.88 ppm (**2**), and showed an excellent correlation with the experimental values. Similarly, the experimental and simulated chemical shifts of methyl protons in both compounds correlated excellently.

A comparison of experimental and computed ^{13}C NMR chemical shift is narrated in Table S3, and an excellent correlation is observed themselves. In the experimental scan of **1**, chemical shifts at 176.8 ppm, 161.2 ppm and 153.1 ppm were assigned to the quaternary carbons C7, C8 and C2 (atomic labeling is in accordance with Fig. 4) respectively, whereas the computed values for these carbons appeared at 186.3 ppm, 172.2 ppm and 162.2 ppm. The experimental aromatic CH signals in **1** appeared at 128.9–128.1 ppm, which agree nicely with the computed values found in 136.5–131.9 ppm range. The chemical shift of CH_2 in **1** (directly attached to aromatic ring) observed at 54.2 ppm correlates nicely with simulated value appeared at 56.7 ppm. The experimental and computed CH_3 value in **1** showed an excellent

Table 1
Some selected X-ray and simulated bond lengths (Å) of **1** and **2**, (Atomic labels are with reference to Fig. 2).

(1)	X-ray	Calc. (B3LYP)	(2)	X-ray	Calc. (B3LYP)
O1–C16	1.207 (2)	1.223	O1–C16	1.208 (2)	1.222
O2–C17	1.240 (3)	1.339	O2–C17	1.195 (18)	1.208
O2–C18A	1.480 (6)	1.444	O3–C17	1.317 (2)	1.337
O3–C17	1.246 (3)	1.207	O3–C18	1.465 (2)	1.455
N1–N2	1.331 (2)	1.333	N1–N2	1.315 (2)	1.310
N1–C8	1.361 (3)	1.376	N1–C7	1.361 (2)	1.361
N1–C7	1.472 (2)	1.475	N2–N3	1.333 (2)	1.333
N2–N3	1.323 (2)	1.310	N3–C8	1.369 (2)	1.375
N3–C9	1.352 (3)	1.361	N3–C9	1.453 (2)	1.474
C1–C6	1.372 (3)	1.401	C1–C2	1.387 (3)	1.403
C1–C2	1.379 (3)	1.398	C1–C6	1.391 (3)	1.405
C1–C7	1.509 (3)	1.516	C1–C7	1.467 (3)	1.470
C2–C3	1.373 (3)	1.396	C2–C3	1.383 (3)	1.395
C4–C5	1.363 (5)	1.397	C3–C4	1.362 (4)	1.395
C5–C6	1.389 (4)	1.393	C4–C5	1.372 (4)	1.397
C10–C11	1.387 (3)	1.405	C5–C6	1.386 (4)	1.392
C10–C15	1.387 (3)	1.403	C7–C8	1.384 (2)	1.403
C11–C12	1.374 (3)	1.392	C8–C16	1.467 (2)	1.464
C12–C13	1.381 (4)	1.397	C9–C10	1.500 (3)	1.517
C13–C14	1.370 (4)	1.395	C10–C11	1.367 (3)	1.398
C14–C15	1.372 (3)	1.395	C10–C15	1.370 (3)	1.401
C16–C17	1.530 (3)	1.539	C11–C12	1.362 (5)	1.396
			C12–C13	1.364 (5)	1.394
			C13–C14	1.357 (4)	1.397
			C14–C15	1.379 (3)	1.393
			C16–C17	1.527 (2)	1.540
			C18–C19	1.463 (3)	1.514

agreement to each other as well. Similarly, the ^{13}C chemical shifts of all carbons in **2** showed excellent agreement to each other. The quaternary carbons C7, C8 and C2 of **2**, appeared experimentally at 177.3 ppm, 160.7 ppm and 152.8 ppm, whereas the simulated signals of these carbons were found at 186.7 ppm, 171.6 ppm and 162.1 ppm. Experimental aromatic (CH) signal of **2** at 134.0–128.0 ppm, showed an agreement with simulated one's at 136.2–131.8 ppm. Similarly, the CH_2 and CH_3 computed and experimental signals showed an excellent correlation.

3.5. Molecular electrostatic potential (MEP)

Molecular electrostatic potential (MEP) mapping in quantum mechanical chemistry is a valuable tool not only to identify the reactive sites in a compound but also helpful to understand the molecular recognition process [27]. It explains the reactivity of chemical system by predicting electrophilic as well as nucleophilic sites inside any molecule [28]. MEP mapping provides the visual understanding of relative polarity [29], and can be defined mathematically by the following expression.

$$V(r) = \sum \frac{Z_A}{|R_A - r|} - \int \frac{\rho(r')}{|r' - r|} dr'$$

Summation ($\sum$) runs over all nuclei, Z_A is charge of nucleus located at distance R_A and $\rho(r')$ is electron density. During MEP mapping, electrophilic and nucleophilic regions are explained by the appearance of different colors, the preferred nucleophilic site is represented by red color, electrophilic site is represented by blue

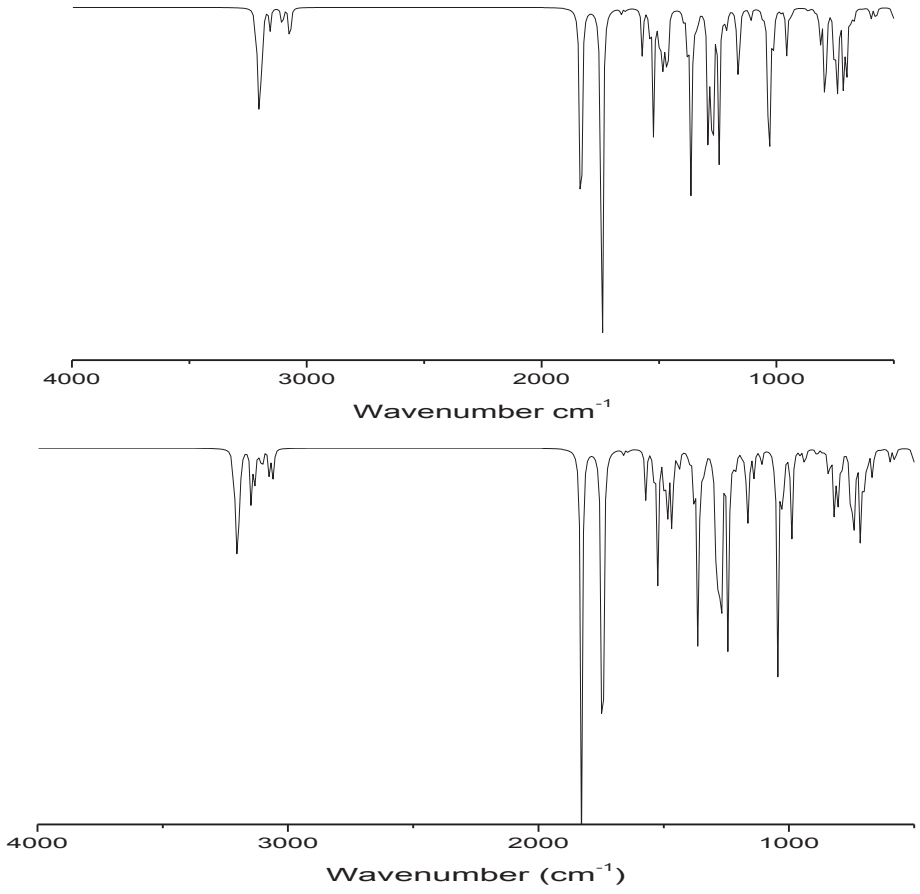

Fig. 5. Simulated vibrational spectra of compound **1** (above) and **2** (below).

Table 2
Experimental and simulated vibrational (cm^{-1}) frequencies of **1** and **2**, (only those simulated values are narrated, those have intensity above 10).

1 Calc. (Intensity)	1 (Exp.)	Assignment	2 Calc. (Intensity)	2 (Exp.)	Assignment
3071(20.8)	–	υ_s, $\upsilon_{as}CH_{arom.}$	3071(21.4)	–	υ_s, $\upsilon_{as}CH_{arom.}$
3069(24.9)	3031	υ_{as}, $\upsilon_sCH_{arom.}$	3069(23.4)	3057	υ_s, $\upsilon_{as}CH_{arom.}$
3062(19.3)	–	υ_{as}, $\upsilon_sCH_{arom.}$	3062(19.4)	–	$\upsilon_{as}CH_{arom.}$
3024(11.0)	–	$\upsilon_{as}Me$	3015(25.4)	3036	$\upsilon_{as}Me$,υ_sCH_2
2974(11.8)	–	υ_sCH_2	3002(17.7)	–	$\upsilon_{as}Me$
			2973(11.7)	2981	υ_sCH_2
2943(23.1)	2954	υ_sMe	2945(14.2)	–	υ_sCH_2
1755(170.5)	1739	υ_sCOOCH_3	2930(13.7)	2937	υ_sMe
1670(246.9)	1687	$\upsilon_sC=O$	1751(182.9)	1741	υ_sCOOCH_3
1505(24.1)	–	$\upsilon_sC=C$	1671(237.6)	1683	υ_sCO
1483(11.6)	1484	$\upsilon_{as}C=C_{arom.}$	1513(23.3)	1537	$\upsilon_sC=C$
1467(62.2)	1455	$\upsilon_{as}C=C_{arom.}$	1483(11.6)	–	$\beta CH_{arom.}$
1434(12.9)	1431	$\upsilon_{as}C=C_{arom.}$	1467(58.7)	1477	$\upsilon_sC=C_{arom.}$
1426(30.6)	–	ρCH_2	1434(13.5)	–	$\beta CH_{arom.}$
1409(48.7)	–	υ_sC-N	1427(28.1)	–	ρCH_2
1328(17.5)	1331	ρN-C-C	1411(43.8)	1453	$\upsilon_sC=N$
1315(14.8)	–	$\beta CH_{arom.}$	1385(12.4)	–	υ_sCH_2-CH_3
1312(87.4)	1311	υ_sC-N	1329(18.9)	–	ρN-C-C
1242(82.6)	1271	$\upsilon_{as}C=N$	1315(14.2)	–	βCH_{arom}
1224(109.6)	1220	$\upsilon_sN=N$	1311(93.3)	1333	υ_sC-N
1198(76.7)	1193	$\upsilon_sC=N$	1240(96.7)	1262	$\upsilon_sC=N$
1122(32.1)	–	τCH_2	1224(125.8)	1224	$\upsilon_sN=N$
1114(16.1)	–	τCH_2	1196(99.6)	1201	$\upsilon_sC=N$
993(118.0)	1015	υ_sO-Me	1123(37.2)	1142	υ_sN-N
975(15.0)	978	βPh	1117(11.5)	–	τCH_2
921(21.6)	927	γPh	1097(12.0)	–	ωMe
783(18.4)	782	υ_sCH_2-Ph	1005(103.3)	1013	υ_sO-Et
764(43.5)	–	$\gamma CH_{arom.}$	987(32.1)	971	βPh
759(17.6)	–	$\gamma CH_{arom.}$	952(44.8)	–	–
724(39.9)	731	$\gamma CH_{arom.}$	810(14.7)	796	$\gamma CH_{arom.}$
711(40.7)	704	$\gamma CH_{arom.}$	787(34.5)	777	υ_sCH_2-Ph
687(20.8)	684	$\gamma CH_{arom.}$	774(22.4)	–	γCH
687(30.0)	664	$\gamma CH_{arom.}$	724(45.8)	730	$\gamma CH_{arom.}$

υ_s, Symmetric treching; υ_{as}, Asymmetric streching; β, In plane bending; γ, Out of plane bending; τ, twisting; ρ, Scissoring; ω wagging.

Table 3
Comparison of experimental and simulated ^{1}H NMR of **1** and **2** (ppm), (Atomic labels are with reference to Fig. 4).

Proton (1)	Exp.	Calc. (B3LYP)	Proton (2)	Exp.	Calc. (B3LYP)
H_{19} (aromatic)	7.47-	8.48	H_{18} (aromatic)	7.45-	8.59
H_{28} (aliphatic)	7.34	8.43	H_{27} (aliphatic)	7.33	8.51
H_{17} (aromatic)	(aromatic	8.21	H_{16} (aromatic)	(aromatic	8.24
H_{32} (aromatic)	protons)	7.81	H_{31} (aromatic)	protons)	7.77
H_{34} (aromatic)		7.70	H_{33} (aromatic)		7.67
H_{22} (aromatic)		7.69	H_{21} (aromatic)		7.66
H_{23} (aromatic)		7.61	H_{20} (aromatic)		7.58
H_{21} (aromatic)		7.55	H_{22} (aromatic)		7.55
H_{33} (aromatic)		7.49	H_{32} (aromatic)		7.54
H_{30} (aromatic)		7.39	H_{29} (aromatic)		7.40
H_5 (CH_2)	5.90	5.90	H_6 (CH_2)	5.88	5.88
H_6 (CH_2)	5.90	5.83	H_5 (CH_2)	5.88	5.88
H_{11} (CH_3)	3.28	3.74	H_{10} (CH_2)	3.71	4.11
H_{10} (CH_3)	3.28	3.62	H_{11} (CH_2)	3.71	3.87
H_{12} (CH_3)	3.28	3.52	H_{40} (CH_3)	0.91	1.56
			H_{42} (CH_3)	0.91	1.47
			H_{41} (CH_3)	0.91	1.18

color and green region represents close to zero potential. The electrostatic potential increases in the order red < orange < yellow < green < blue. Molecular electrostatic potential mapping of **1** and **2** was simulated at the same level of theory as used to obtain energy minima structures and surfaces are shown in the (Fig. 6).

It is clear from MEP surfaces that both compounds **1** and **2**, are nucleophilic in nature and negative region is concentrated on triazole and oxalyl moieties, and these are preferred sites for electrophiles or positive charge containing species. MEP value was ranged from −0.0496 a. u. to 0.0496 a. u. for **1** and −0.0498 a. u. to 0.0498 a. u. for compound **2**.

3.6. Frontier molecular orbitals (FMOs) analysis

The FMOs analysis play has a vital role to understand the absorptions, electronic as well as optical properties of chemical compounds [30]. The energy gap between the highest occupied orbital (HOMO) and lowest unoccupied orbital (LUMO) is very important in term of explaining the chemical behavior of any compound. Small HOMO–LUMO energy gap means high chemical reactivity, low kinetic stability, and vice versa [31]. The surfaces of the HOMO and LUMO orbitals were simulated at the B3LYP/6-31G (d, p) level of theory in gas phase and are shown in Fig. 7.

As it is reflected from Fig. 7, that the electronic cloud in HUMO of

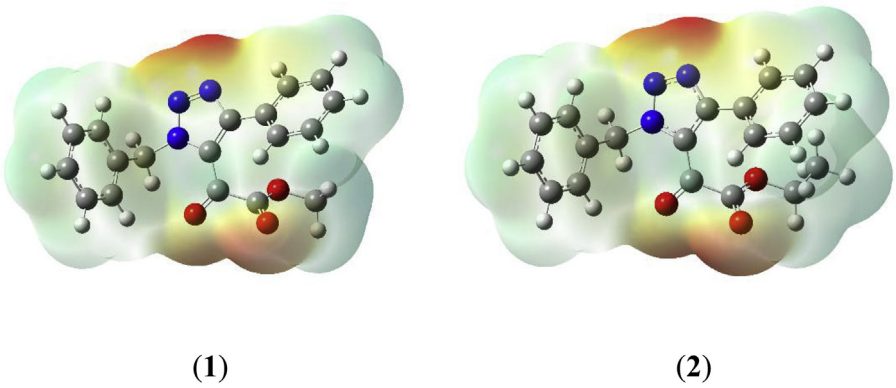

Fig. 6. MEP surfaces of **1** and **2** at B3LYP/6-31G (d, p) level of DFT.

both **1** and **2** is mainly localized on aromatic and triazole moieties, whereas LUMO electrons are mainly located on the aromatic ring directly attached to triazole and oxalyl moiety. The energy of HOMO orbital corresponds to the ionization potential (I. P) and energy of LUMO orbital corresponds to the electron affinity (E. A.). FMOs analysis of **1** revealed that there are total 84 filled orbitals and energy difference between HOMO-LUMO is 4.216 eV. Whereas compounds **2** have 88 filled orbitals and the energy difference between HOMO-LUMO is equal to 4.24 eV. HOMO-LUMO energy difference revealed that both compounds are highly reactive and kinetically less stable, furthermore both compounds have almost same energy difference (ΔE) therefore have same sort of reactivity.

3.7. Brine shrimp cytotoxic lethality assay

Brine shrimp cytotoxicity assay is a simple and inexpensive methodology employed for the detection and isolation of bioactive compounds with significant cytotoxic potential. This assay has been employed successfully for the exploration of commercially important bioactive compounds. In the present study, compound **2** was more potent (LC_{50} 12.58 μg/ml) as compared to compound **1** (LC_{50} 13.3 μg/ml) (Table 4). The degree of lethality was found to be directly proportional to descending concentration of extract as highest mortality (100%) was found at maximum concentration (300 μg/ml), minimum mortality was found at the lowest concentration (Fig. 8). These results can be associated with the previous findings in which bis-triazole derivatives depicted high mortality percentage (50%) at concentrations ranging from 50 to 150 μg/ml [32]. However, on the contrary findings of another report suggest the less cytotoxic behavior of various thiazolo- and 1, 2, 3-thiadiazolo-4-*H*-1,2,4-triazoles derivatives against brine shrimps at concentrations of 100 and 10 μg/ml [33]. Previous documents propose that due to commercial availability and bearing most sensitive biological system, newly hatched larvae of *A. salina* L., is one of the most suitable living models to evaluate the bioactivity of wide variety of samples. It is apparent from the present study that

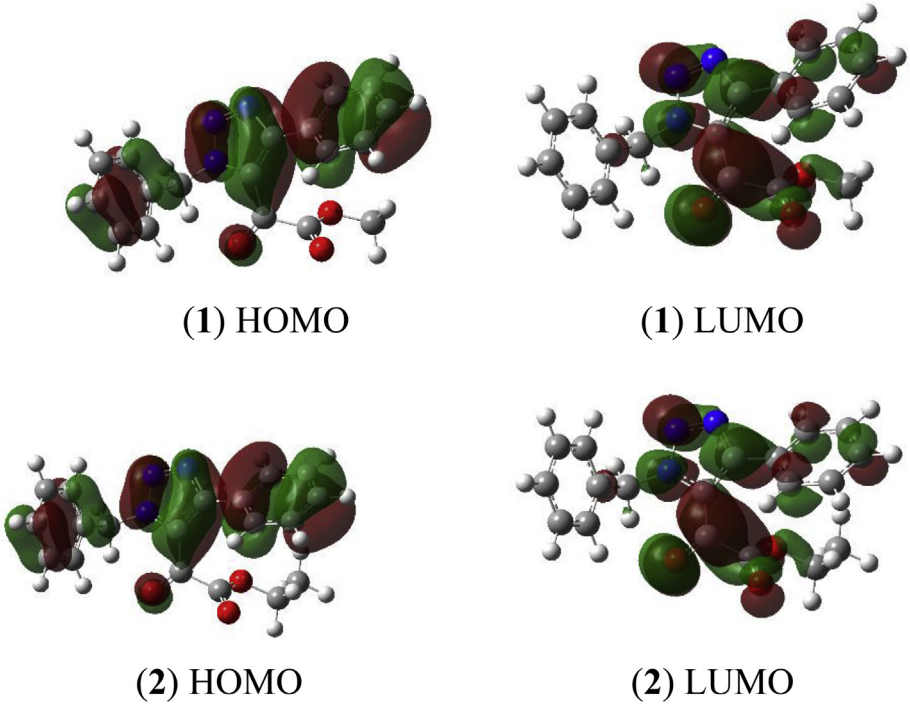

Fig. 7. HOMO-LUMO surfaces of both compounds **1** and **2**.

Table 4
Brine shrimp lethality assay of both compounds **1** and **2**.

Compound	Brine shrimp lethality assay (concentration μg/mL)						
	% Mortality						LC_{50}
	300	100	33.3	11.1	3.7	1.3	
1	100 ± 1.21	90 ± 0.98	70 ± 0.72	45 ± 0.62	15 ± 0.56	0	13.3 ± 0.45
2	100 ± 1.18	100 ± 1.02	90 ± 0.88	40 ± 0.59	15 ± 0.60	5 ± 0.43	12.58 ± 0.39

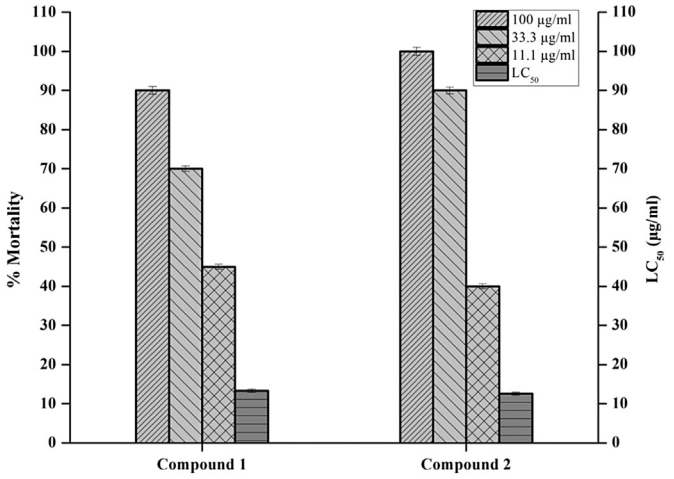

Fig. 8. LC_{50} values of both compounds **1** and **2** at different concentrations.

cytotoxicity profile of the tested compounds is higher even at lower concentrations. This shows that tested compounds have very strong capability of interaction with the model biological system. Most of the drugs exert their pharmacological effects by interaction with the biological system through receptors, subcellular components and enzyme. So, this study hypothesize that further detailed investigation of these compounds can explore the potential useful pharmacological effects of these compounds. This is strongly supported by Silva et al. (2009) who described that brine shrimp assay had served the purpose of exploration of numerous pharmacological properties of natural products as well as synthesized compounds including antimicrobial, antitumor, antifungal, antimalarial, molluscicidal, larvicidal and insecticidal activities, eventually leading said compounds to serve as potential candidate for the preparation of effective medicines against various diseases [34,35].

4. Conclusions

Two new triazoles has been synthesized by using the click one pot three components synthesis strategy in more than 91% yields. Structures of both triazoles were characterized by using various spectroscopic techniques and the structures were confirmed through X-ray crystallographic studies. X-ray diffraction analysis revealed that the geometries of both compounds are stabilized via $H_7\cdots O_1$ (compound **1**) and $H_{19}—N_1$, $O_3—H_9$ (compound **2**) hydrogen bonding interactions. DFT investigations proved very strong correlation between X-ray diffraction as well as simulated results. For **1**, deviation in bond lengths observed in the range 0.002–0.099 Å and 0.1–5.6° in bond angles. Similarly, for **2**, observed deviation is 0.00–0.034 Å (bond lengths) and 0.0–3.3° (bond angles). Simulated vibrations were scaled by using scaling factors of 0.958 (above 1700 cm^{-1}) and 0.9627 (below 1700 cm^{-1}) in order to minimize the theoretical error, and showed an excellent correlation with experimental values. MEP mapping revealed that both compounds are nucleophilic in nature and negative region is concentrated on triazole and oxalyl moieties, and these are preferred site for electrophiles. Charge separation ranged from −0.0496 a. u. to 0.0496 a. u. for **1** and −0.0498 a. u. to 0.0498 a. u. for compound **2**. FMOs analysis showed that both compounds are kinetically less stable having low HOMO-LUMO energy gap i. e. equal to 4.24 eV. Brine shrimp cytotoxicity assay proved that **2** was more potent (LC_{50} 12.58 μg/ml) as compared to **1** (LC_{50} 13.3 μg/ml) at nontoxic level of concentration.

Acknowledgments

The authors are highly thankful to Higher Education Commission Pakistan (HEC) for financial support (Grant no. 20-3013/NRPU/R&D/HEC/14/525).

Appendix A. Supplementary data

Supplementary data related to this article can be found at http://dx.doi.org/10.1016/j.molstruc.2015.11.010.

References

[1] P. Thirumurugan, D. Matosiuk, K. Jozwiak, Chem. Rev. 113 (2013) 4905–4979.
[2] C. Besanceney-Webler, H. Jiang, T. Zheng, L. Feng, D. Soriano del Amo, W. Wang, L.M. Klivansky, F.L. Marlow, Y. Liu, P. Wu, Angew. Chem. Int. Ed. Engl. 50 (2011) 8051–8056.
[3] H.C. Kolb, M. Finn, K.B. Sharpless, Angew. Chem. Int. Ed. Engl. 40 (2001) 2004–2021.
[4] H.C. Kolb, K.B. Sharpless, Drug Discov. Today 8 (2003) 1128–1137.
[5] J.E. Moses, A.D. Moorhouse, Chem. Soc. Rev. 36 (2007) 1249–1262.
[6] V.V. Rostovtsev, L.G. Green, V.V. Fokin, K.B. Sharpless, Angew. Chem. Int. Ed. Engl. 114 (2002) 2708–2711.
[7] V.D. Bock, H. Hiemstra, J.H. Van Maarseveen, Eur. J. Org. Chem. 1 (2006) 51–68.
[8] N.T. Pokhodylo, Top. Heterocycl. Chem. Springer-Verlag Berlin Heidelberg (2014) 269–324.
[9] B. Wang, M.N. Ahmed, J. Zhang, W. Chen, X. Wang, Y. Hu, Tetrahedron Lett. 54 (2013) 6097–6100.
[10] M.N. Arshad, A.M. Asiri, K.A. Alamry, T. Mahmood, M.A. Gilanid, K. Ayub, A.S. Birinji, Spectrochim. Acta Part A 142 (2015) 364–374.
[11] T. Ur Rahman, M. Arfan, T. Mahmood, W. Liaqat, M.A. Gilani, G. Uddin, R. Ludwig, K. Zaman, M.I. Choudhary, K.F. Khattak, K. Ayub, Spectrochim. Acta Part A 146 (2015) 24–32.
[12] T. Ur Rahman, G. Uddin, R. Un Nisa, R. Ludwig, W. Liaqat, T. Mahmood, G. Mohammad, M.I. Choudhary, K. Ayub, Spectrochim. Acta Part A 148 (2015) 375–381.
[13] E.C. Woon, A. Dhami, M.F. Mahon, M.D. Threadgill, Tetrahedron 62 (2006) 4829–4837.
[14] K.A. Gschneidner, L. Eyring, G.H. Lander, Handbook on the Physics and Chemistry of Rare Earths, 32, Elsevier, 2002.
[15] G.M. Sheldrick, SHELXS, SHELXL, ActaCryst. A64 (2008) 112.
[16] M.J. Frisch, G.W. Trucks, H.B. Schlegel, G.E. Scuseria, M.A. Robb, J.R. Cheeseman, G. Scalmani, V. Barone, B. Mennucci, G.A. Petersson, H. Nakatsuji, M. Caricato, X. Li, H.P. Hratchian, A.F. Izmaylov, J. Bloino, G. Zheng, J.L. Sonnenberg, M. Hada, M. Ehara, K. Toyota, R. Fukuda, J. Hasegawa, M. Ishida, T. Nakajima, Y. Honda, O. Kitao, H. Nakai, T. Vreven, J.A. Montgomery Jr., J.E. Peralta, F. Ogliaro, M. Bearpark, J.J. Heyd, E. Brothers, K.N. Kudin, V.N. Staroverov, R. Kobayashi, J. Normand, K. Raghavachari, A. Rendell, J.C. Burant, S.S. Iyengar, J. Tomasi, M. Cossi, N. Rega, J.M. Millam, M. Klene, J.E. Knox, J.B. Cross, V. Bakken, C. Adamo, J. Jaramillo, R. Gomperts, R.E. Stratmann, O. Yazyev, A.J. Austin, R. Cammi, C. Pomelli, J.W. Ochterski, R.L. Martin, K. Morokuma, V.G. Zakrzewski, G.A. Voth, P. Salvador,

J.J. Dannenberg, S. Dapprich, A.D. Daniels, Ö. Farkas, J.B. Foresman, J.V. Ortiz, J. Cioslowski, D.J. Fox, Gaussian 09, Revision C.01, Gaussian, Inc., Wallingford CT, 2010.
[17] D. Roy, K. Todd, M. John, Gauss View, Version 5, Semichem, Inc., Shawnee Mission, KS, 2009.
[18] I.U. Haq, N. Ullah, G. Bibi, S. Kanwal, M.S. Ahmad, B. Mirza, Iran. J. Pharm. Res. 11 (2010) 241–249.
[19] M.N. Ahmed, S. Hameed, K.A. Yasin, I. Arshad, I. ul-Haq, S. Zafar, M.N. Tahir, Chin. J. Struct. Chem. 33 (2014) 1666–1672.
[20] M.N. Ahmed, I. Arshad, W. Bo, S. Hameed, B.A. Khan, K.A. Yasin, M.M. Naseer, Chin. J. Struct. Chem. 33 (2014) 1749–1756.
[21] N. Sundaraganesan, S. Ilakiamani, H. Saleem, P.M. Wojciechowski, D. Michalska, Spectrochim. Acta A 61 (2005) 2995–3001.
[22] C.S.C. Kumar, H.K. Fun, C. Parlak, L. Rhyman, P. Ramasami, M. Tursun, S. Chandraju, C.K. Quah, Spectrochim. Acta Part A 132 (2014) 174–182.
[23] V.D. Vitnik, Z.J. Vitnik, N.R. Banjac, N.V. Valentic, G.S. Uscumlic, I.O. Juranic, Spectrochim. Acta A 117 (2014) 42–53.
[24] A. Teimouri, A.N. Chermahini, K. Taban, H.A. Dabbagh, Spectrochim. Acta A 72 (2009) 369–377.
[25] J.B. Bhagyasree, H.T. Varghese, C.Y. Panicker, C. Van Alsenoy, A.A. Al-Saadi, M. Dolezal, J. Samuel, Spectrochim. Acta Part A 137 (2015) 193–206.
[26] P.R. Rablen, S.A. Pearlman, J. Finkbiner, J. Phys. Chem. A 103 (1999) 7357–7363.
[27] E. Scrocco, J. Tomasi, Adv. Quantum Chem. 11 (1978) 115–121.
[28] F.J. Luque, J.M. Lopez, M. Orozco, Theor. Chem. Acc. 103 (2000) 343–345.
[29] P. Politzer, P.R. Laurence, K. Jayasuriya, Environ. Health Perspect. 61 (1985) 191–202.
[30] Z. Demircioglu, C. Albayrak, O. Buyukgungor, Spectrochim. Acta A 128 (2014) 748–758.
[31] I. Fleming, Frontier Orbitals and Organic Chemical Reactions, Wiley, London, 1976.
[32] M. Al-Amin, M.R. Islam, Bangladesh J. Pharmacol. 1 (2006) 21–26.
[33] A.R. Jalilian, S. Sattari, M. Bineshmarvasti, A. Shafiee, M. Daneshtalab, Arch. Pharm. 333 (2000) 347–354 (Weinheim).
[34] J. Silva, J. Nichols, T.W. Theunissen, G. Guo, A.L. Van Oosten, O. Barrandon, J. Wray, S. Yamanaka, I. Chambers, A. Smith, Cell 138 (2009) 722–737.
[35] I.-U. Haq, B. Mirza, T.P. Kondratyuk, E.-J. Park, B.E. Burns, L.E. Marler, J.M. Pezzuto, Pharm. Biol. 51 (2013) 316–328.